

Characterizing fjord oceanography near tidewater glaciers Kronebreen and Kongsvegen, in Kongsfjorden, Svalbard

Daksha M. Rajagopalan

with

Mary-Louise Timmermans (Yale U. G & G),
Ross Powell (Northern Illinois U.),
and Julie Brigham-Grette (U. Mass - Amherst)

Physics Senior Project
Department of Physics
Yale College

7 May 2012,

Modified 12 May 2012

Abstract

In recent years, warmer Atlantic-origin waters have intruded into Svalbard's west-coast fjords. To predict the effects of the TAW (transformed Atlantic water) intrusion on the ice margin of tidewater glaciers, a detailed understanding of fjord circulation is important. While the general fjord circulation of Kongsfjorden, Svalbard, is well-understood, water masses closest to the ice margin – and directly responsible for sub-marine glacial melt – are more difficult to study. To characterize the water masses and interpret fjord circulation at the calving-fronts of glaciers Kronebreen and Kongsvegen, Svalbard, oceanographic fieldwork was conducted along five primary transects, with the view to account for tidal influences as well. CTD (conductivity, temperature, depth) devices with attached OBS (relative turbidity) sensors were used to collect data that range from 200 m to 1.7 km from the ice face, between 22 Jul and 6 Aug 2011. Current velocities were also estimated using drogues constructed while in Svalbard. The data show significant variability in the water column stratification between just days. In addition to the tidal cycle, winds and other factors also appear to play a major role in glacial discharge streams and circulation. A comparison with data collected in the same region in Jul 2005 (by Trusel et al. 2010) show the 2011 Intermediate Water (IW) at depth to be warmer than the 0° local water (LC) that was observed at comparable depths in 2005. These two layers lie above the TAW and may be warmer as a result of convection with increased TAW waters. Increased intrusion of Atlantic-origin waters after 2005 are likely to have warmed the waters in the inner fjord of Kongsfjorden, indicating that the ice margin of tidewater glaciers in Kongsfjorden are susceptible to heat fluxes from North Atlantic water intrusions.

Table of Contents

Phys 472 Course Report(*coursereport.pdf*)

1. Introduction
 - 1.1 Motivation
 - 1.2 This Project and Research Question
 - 1.3 Fieldsite
2. Methods
 - 2.1. In field
 - 2.2. Processing and this academic year
3. Results
 - 3.1. Water Column Structure
 - 3.2. Daily Variability
 - 3.3. Interannual Variability
4. Conclusions and Future Directions
5. References
6. Acknowledgements

Appendix A: 2011 Svalbard REU Oceanographic Data Report

1. Introduction to the Fieldwork(*AppendixA1.pdf*)
2. Drogue Data
 - 2.1. Overview
 - 2.2. Surface
 - 2.3. 20 m depth
 - 2.4. 40 m depth
 - 2.5. 50 m depth
3. CTD and turbidity Data
 - 3.1. Pre-Fieldwork: Instrument Specs and Calibration
 - 3.1.1. Specs for Gretel
 - 3.1.2. Specs for Hans
 - 3.1.3. Config Files for Gretel
 - 3.1.4. Config Files for Hans
 - 3.2. Fieldwork: Descent Rates and Resolution
 - 3.3. Post-Fieldwork: Data Processing
 - 3.4. Profiles.....(*Appendix A2.pdf*)
 - 3.5. Chronological Transect Overview.....(*Appendix A3.pdf*)
 - 3.6. Water Mass Classification
 - 3.7. Transects
 - 3.8. Delta Transects
 - 3.9. Upwelling Transects

- 3.10. Transverse Transects
- 4. Subglacial Stream Upwelling Velocity.....(*Appendix A4.pdf*)

Appendix B: Interannual Data.....(*AppendixB.pdf*)

- 1. Appendix B: Past years' CTD Data
 - 1.1. 2005 Data: Introduction
 - 1.2. 2005 Data: Transects

Appendix C: Tidal Data.....(*AppendixC.pdf*)

- 1. Appendix C: Tidal Data

Appendix D: Meteorological Data.....(*AppendixD.pdf*)

- 1. Appendix D: Meteorological Data
 - 1.1. 2011 Temp. Precipitation, Wind Data – Daily Averages
 - 1.2. 2011 Meteorological Data from eKlima
 - 1.2.1. Hourly met data.....(*2011Methourly.pdf*)
 - 1.2.2. 6-hourly data.....(*AppendixD.pdf*)
 - 1.3. 2005 Meteorological Data from eKlima

Appendix E: MATLAB Code.....(*AppendixE.pdf*)

- 1. Appendix E: Matlab Code
 - 1.1. Code I Wrote
 - 1.1.1. descent.m
 - 1.1.2. findminmax.m
 - 1.1.3. createODV.m
 - 1.1.4. droguedistance.m
 - 1.1.5. createArrayStruct.m
 - 1.1.6. createArrayStruct2005.m
 - 1.2. Code Written By Others
 - 1.2.1. ltp_make_odv.m
 - 1.2.2. Pos2dist.m
 - 1.2.3. Gsw_p_from_z.m
 - 1.2.4. Gsw_enthalpy_SSO_0_CT25.m
 - 1.2.5. Gsw_specvol_SSO_0_CT25.m

1. Phys 472 Course Report

Contents

1	Introduction	1
1.1	Motivation	1
1.2	This Project and Research Question	2
1.3	Fieldsite	3
2	Methods	4
2.1	In field	4
2.2	Processing and this academic year	6
3	Results	7
3.1	Water Column Structure	8
3.2	Daily Variability	8
3.3	Interannual Variability	13
4	Conclusions and Future Directions	13
5	References	16
6	Acknowledgements	18

1 Introduction

1.1 Motivation

The Arctic is particularly sensitive to, and important in, climate change. Glacial melt increases freshwater input (affecting ocean circulation patterns), results in sea-level rise, and decreases the earth's albedo (or reflectivity, which generates a positive-feedback for further global warming). Thus it is important to understand how glaciers melt.

Tidewater glaciers (see Figure 1), which typically terminate in fjords, lose ice through three primary mechanisms: surface, englacial, and subglacial meltwater streams, calving (when a chunk of ice breaks off the glacier and falls into the fjord waters), and submarine melt at the ocean-ice interface. Both calving rates and submarine glacial melt are influenced by local oceanographic conditions. As fjord waters interact with the ice, they can undercut a glacier, making it more prone to calving (Benn et al. 2007). Warmer inner fjord waters have also been observed to increase the submarine melt rates of tidewater glaciers in Alaska and Greenland (see Motyka et al. 2003, Rignot et al. 2010). Recent research in Greenland has shown that glacial surges (or sudden acceleration of the glacier into the fjord) can be triggered by an anomalous influx of warmer subsurface waters (Holland et al. 2008). Understanding the oceanography near the ocean-ice interface is thus particularly important and timely.

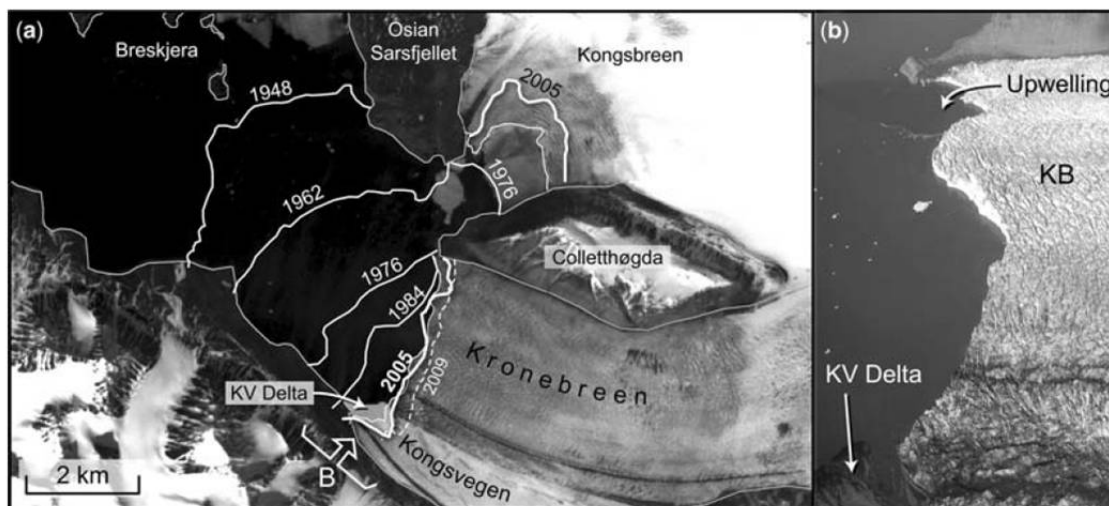


Figure 1: Tidewater glaciers Kronebreen and Kongsvegen terminate in the fjord Kongsfjorden. a) Note the receding ice margin of the fieldsite (Kronebreen-Kongsvegen glacial complex) from 1948 to 2009, b) an aerial view of the two glaciers, from Jul 2005 (Source: Trusel et al., 2010).

Fjords along the western coast of Svalbard are particularly prone to warmer water intrusions since waters from the gulf stream flow adjacent to Svalbard as the West Spitsbergen Current (See Figure 2). Recently, warmer North Atlantic Water (bringing heat from the gulf stream) has been intruding farther into the fjords of west Svalbard, altering the oceanography and possibly affecting winter sea ice cover (e.g. Isfjorden in 2011: see Nilsen et al. 2011; Kongsfjorden in 2006: see et al. 2007, Willis et al. 2008). In 2006, biological oceanographers discovered a change in the phytoplankton community in Kongsfjorden (the fieldsite for our project) driven by a sudden and anomalous influx of warmer Transformed Atlantic Water (TAW), a mixture of Arctic-type and Atlantic-type water (Willis et al. 2008).

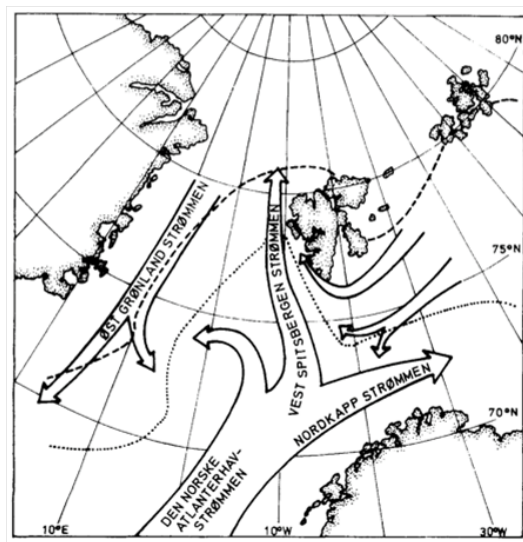


Figure 2: The main current system around Svalbard (Svalbard is roughly in the center of this map, above mainland Norway and east of Greenland). Note that the warmer North Atlantic stream continues along the west coast of Svalbard as the West Spitsbergen Current (WSC) (Source: Hasle and Heimdal, 1998).

1.2 This Project and Research Question

In order to better understand ice loss and whether warmer North Atlantic waters can penetrate deep enough to impact glacial melt, the primary question motivating this research project is: what factors are driving ocean circulation close to the glacier margins?

This project combined fieldwork with data processing and analysis. The fieldwork was conducted over the summer as part of an REU program, and my work over the academic

year has mostly involved processing and organizing the data, with some interpretation of the data.

1.3 Fieldsite

Notably, Kongsfjorden does not have a sill (a rise in the bathymetry at the mouth of the fjord, at the terminus of the previous glaciation), making it more vulnerable to the ocean waters (Svendsen et al. 2002). It is known that Atlantic water penetrates into Kongsfjorden at 75-100m depth in the spring and summer, likely due to this lack of a fjord sill (Elverhøi et al. 1983). Intrusions of warmer Atlantic water in early 2006 were also caused by large-scale atmospheric circulation patterns (Cottier et al. 2007). The question driving this project is whether this warmer Atlantic water—or the heat from this water—penetrates all the way to the ice face (see Figure 3).



Figure 3: The fieldsite (Source: Svendsen et al. 2002. Kongsfjorden and Krossfjorden are on the western coast of Svalbard. The inner fjord waters – and the fieldsite for this study – are circled in red.)

Current research suggests that the oceanography closest to the ice face in Kongsfjorden is driven by three factors: 1) waters from the outer fjord, 2) local wind conditions, and 3) glacial discharge streams, likely to be most affected by tidal cycles (Svendsen et al. 2002). The fieldsite has two glacial meltwater discharges: a surface delta overflow from Kongsvegen and a turbid upwelling plume from Kronebreen (see Figure 6 for a map, and Figures 4 and 5 for explanations). These glacial meltwater discharge streams are also known to exhibit

variability on an interannual scale; Kongsfjorden's upwelling, for example, moved about 500 m north between 1987 and 2009 (Kehrl et al. 2011).

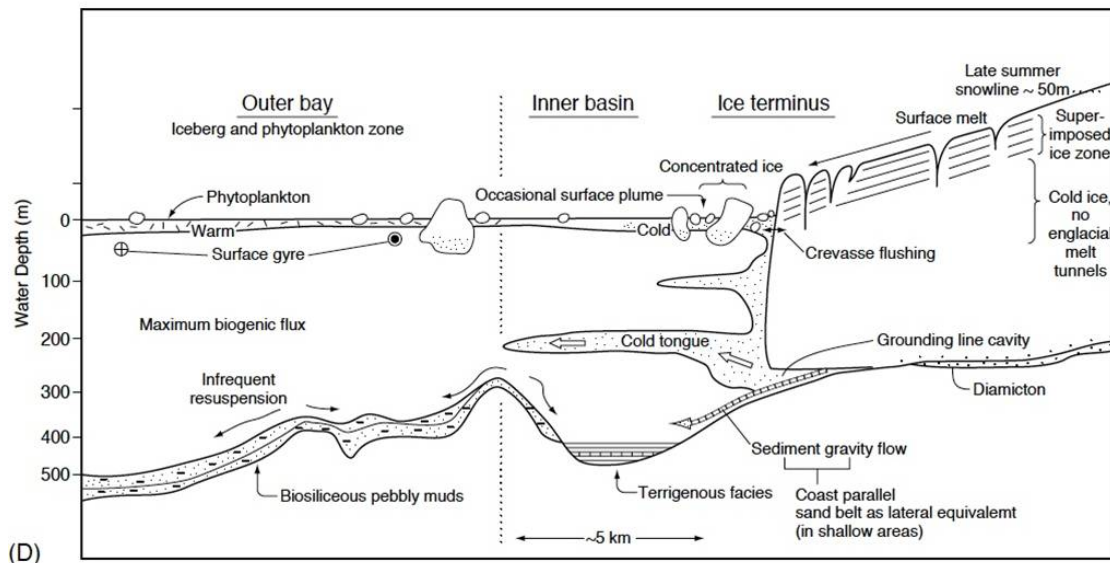


Figure 4: A schematic diagram of a fjord (Source: Powell, 2003). On the far right is the cross-section of a glacier. Note the meltwater (cold tongues and occasional surface plumes) that come from the glacier. Sometimes these can be surface discharges (such as the delta discharge from Kongsvegen coming from the southern shore of Kongsfjorden) and sometimes these can be submarine meltwater streams that rise turbulently to form an upwelling (such as from Kronebreen, also see Figure 5). The fieldsite for our project lies within the inner basin of Kongsfjorden.

2 Methods

2.1 In field

For more details on the instrument specifications, calibrations, and field techniques, please see Appendix A: Data Report.

The sampling strategy was designed to investigate the variability in the meltwater discharges and inner basin oceanography over the scale of days. In particular, we wanted to understand tidal variability in the discharge streams. We used two CTD (Conductivity, Temperature, Pressure) devices that we nicknamed Hans and Gretel (both manufactured by Seabird) with attached OBS (relative turbidity, or sediment concentration) sensors,

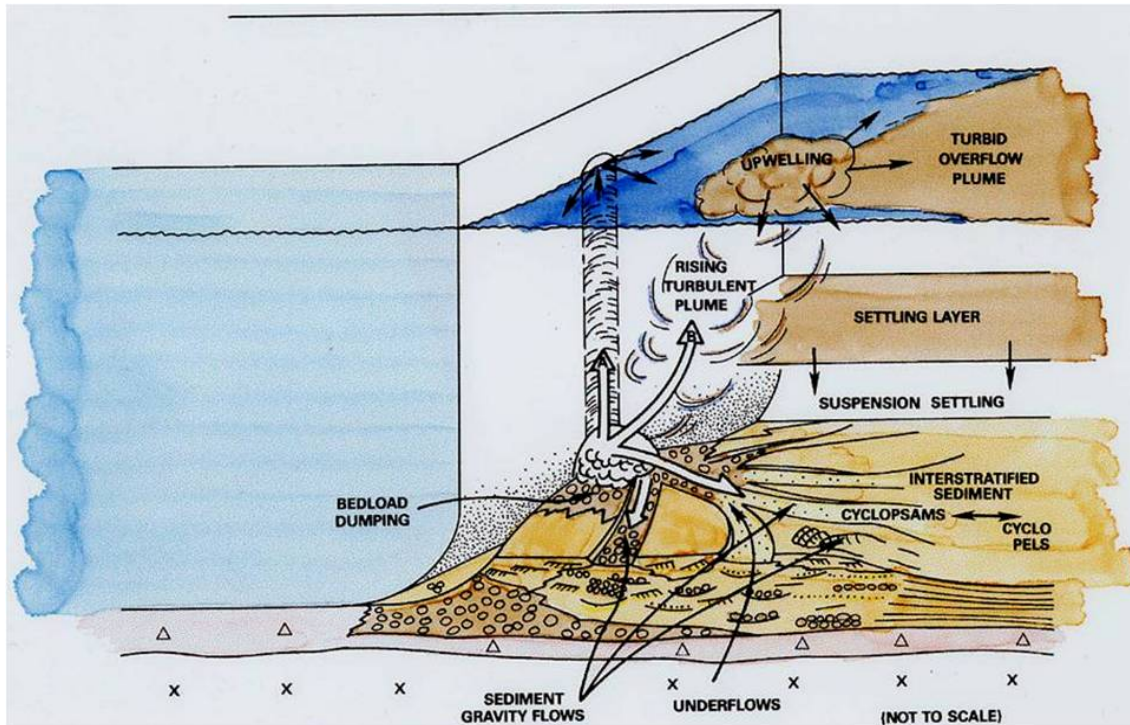


Figure 5: An upwelling plume (Source: Powell, 1981). As an englacial meltwater stream exits into the inner basin at depth, it may rise turbulently (since it is less saline and more buoyant than the ambient fjord waters) to form a surface plume. This is known as an upwelling, and the inner basin of Kongsfjorden has an upwelling plume from Kronebreen. While in the field, we were able to identify the plume by the color difference in the water, and the specific site of the upwelling as where the birds dive to feed, for we were told that the turbulent and fresh water stuns the krill.

and we sampled across five primary transects (see Figure 6). Each CTD cast involved raising and lowering the device using a hand-operated winch. We took a total of 130 CTD casts between 22 Jul and 6 Aug 2011. While in Ny Ålesund (the research village we were staying at) I also used Seabird's SBE Data Processing unit to convert and import the data into MATLAB, and then used MATLAB to make some rudimentary transect plots. After looking at these plots, we also decided to estimate current velocity at depth, and Julie constructed drogues (or drifter buoys with attached 'sails' at depth) for this purpose.

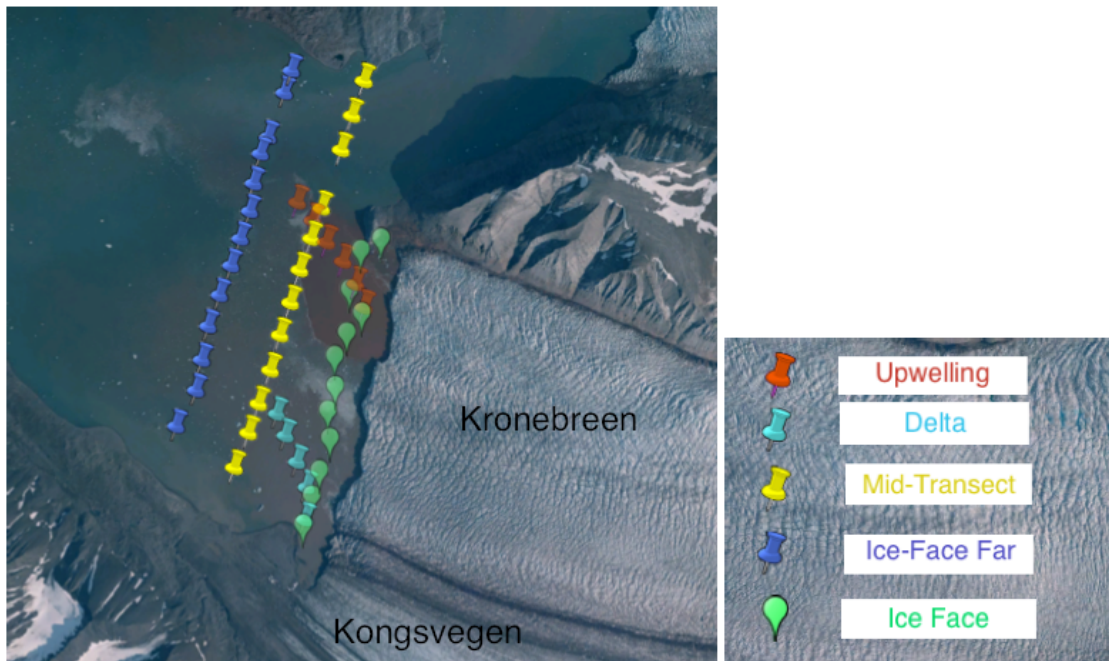


Figure 6: The five primary transects we sampled across. Delta and Upwelling were conducted several times (8 and 6 times, respectively), to capture the different times of the tidal cycle, and the other three (Ice Face, Mid-Transect, and Ice Face Far) were collected to increase the spatial resolution of the data.

2.2 Processing and this academic year

I spent a good part of last semester and this semester further processing data. First I imported the data into MATLAB, built an array of structures, and then used a routine written by my advisor, Mary-Louise, to export all the data as a text file. I then imported the text file in Ocean Data View v. 4.42 (ODV), where I plotted each station (see Appendix A). After doing that, I spent the rest of last semester manually removing spikes in the

data (some due to equipment malfunction, some due to turning on the CTD while it was still above water, some due to 'hitting bottom' and clogging the salinity chamber with sediment). Hans had a lot more spikiness than Gretel. After compiling this into a data report and inserting θ -S diagrams (θ , or potential temperature is frequently plotted against salinity by oceanographers, to characterize water masses. These plots are commonly referred to as 'T-S plots'), we noticed that the T-S plots had lots of loops. Gretel had a lot more loopiness than Hans. Loops on T-S plots are unrealistic in this case since loops connote an instability (and overturning) in the water column. I learned that loops on T-S plots more commonly indicate that the temperature and salinity channels are not quite aligned (i.e. a temperature and salinity sample at a given 'pressure' are not really measuring the same pressure due to the workings of the internal sensors and their dependence on external factors like descent rates). So I went back to Seabird's Data Processing unit (that I had used in the field), read up on recommended alignments for the two different CTD devices, and performed some alignment (details in Appendix A). I noticed that the SBE Data Processing unit had several functions I had not paid attention to while in Ny Ålesund, and I used some of these to wild-edit (remove spikes) and bin-average (by 1 db pressure) the data.

If I were doing this project again, I probably would not spend as much time processing data. Wild-editing and meter-averaging the data to begin with would have been more than sufficient for these purposes. The loopiness was significant (I advanced the channels on the order of $0.5s$, and with an average descent rate of $0.37 \frac{m}{s}$, this yields a misalignment on the order of $20cm$) and there is still room for better alignment of these data (so perhaps a maximum misalignment on the order of a meter), but the loopiness is still not so important for this project since we are interested in large-scale oceanographic structures. Once the data were meter-averaged, and re-imported via MATLAB back into ODV, there were far fewer spikes to manually remove. Next I made transect plots and determined a good range to plot all the data on. Lastly, while rereading Luke Trusel's 2010 paper, I realized that we had observed much warmer water in 2011 than he had in 2005, so I requested his data set, and then processed that data set as well (using a combination of SBE Data Processing, MATLAB, and ODV once more), and then plotted transects of the 2005 data as well (see Appendix B).

The main contribution of my work this year has probably been to produce a relatively clean data set of the inner fjord water column structure in Kongsfjorden on the scale of tidal cycles.

3 Results

For full details, please see Appendix A: Data Report. In addition to more details on the water column structure, Appendix A also includes the results from the drogues and a preliminary subglacial stream discharge velocity calculation.

3.1 Water Column Structure

The general water column structure consists of a relatively cool and fresh surface overflow (SO) between 1 m to 5 m deep (deeper in the upwelling region, shallower in the delta region), which rests upon the surface water (SW). The SW extends to a depth approximately between 25 to 40m. The observed SW in the fieldsite is warmer than formerly classified in Kongsfjorden (compare transects in Appendix A with the table, Classification of Water Masses (after Svendsen et al. 2002, Cottier et al. 2005, Trusel et al. 2010), also in Appendix A). Under the SW lies the Intermediate Water (IW). In most of the casts, the IW extends all the way to the fjord bottom. In few casts, we see the presence of cold local water (LC $< 1^{\circ}\text{C}$) (which in the outer bay of the fjord is known to lie above the warm TAW). Where the LC is present, it is no shallower than 65 m depth. It is more common in the Upwelling transects, and LC is also present in Ice Face Far and Mid-Transect but not in Ice Face (indicating that its origin is indeed from the outer fjord, for it is present at depth, farther from the shore and closer to the center of the fjord).

While there is some variability in the water column structure between different days, the delta transects and upwelling transects have particular turbidity structures as well (see Figures 7 and 8). The two leftmost casts in Upwelling A exhibit a relative turbidity maximum at about 30 m depth, which corresponds with a dip in salinity value and an increase in temperature value at the same depth, indicative of an interflow from the glacial meltwater stream. In Delta D, notice the relative turbidity maximum that fluctuates but lies somewhere between 20 to 40 m depth as the casts move away from the glacier, roughly corresponding with the thermocline at 30 m. This indicates a settling-out of the sediment from the turbid delta overflow. In general, sediment settles out into a layer across the delta transects, at the boundary between the SO and the SW (though Delta B and Delta G, both taken at flood-tide have more complicated turbidity structures). The upwelling region exhibits an interflow, but there is variability in the strength and depth of the interflow as well. The upwelling interflow might extend as far as 1.7 km from the ice face, and the delta settling-out layer definitely extends farther into the fjord (see Figure 9).

3.2 Daily Variability

Most of the daily variability in the water column occurs in the upper 26 m (at $\sigma < 26.5$, where σ is used by oceanographers to express seawater density and its units are $\frac{\text{g}}{\text{L}}$ *in excess of 1 kg*). Particularly, cooler surface waters were present the first two days of fieldwork (22 JUL and 23 JUL), but the following days reveal warmer surface waters on average. While tides were expected to play a major role in circulation and the corresponding water column stratification, tidal influences do not account for all the variability that is seen in the upper water column. For example, compare Delta B and Delta G, both of which are taken at flood-tide (See Figure 10). The intermediate water (IW) starts at 27 m in Delta B and at 49 m in Delta G (indicated by the 34 psu isohaline). The surface water (SW) is

Upwelling A



Delta D



Figure 7: Here are the locations of the two transects in Figure 8

much deeper (about 30m) and warmer ($> 4^{\circ}C$) in Delta G, while Delta B has a thinner and much cooler SW layer (top 20m, around $3^{\circ}C$), which is cooler than the subsurface temperature maximum at 25m. The meteorological station at Ny Ålesund (See Appendix D) shows the air temperatures are similar ($6.1^{\circ}C$ and $7.2^{\circ}C$ respectively) and both days are overcast, though Delta B is preceded by a night of fog. The meteorological station records wind data at the time of Delta B and Delta G as an easterly at $3.2 \frac{m}{s}$ and as blowing from the NNW at $4.6 \frac{m}{s}$, respectively. If these wind conditions are assumed to hold about 11 km upfjord, then at Delta B, an easterly wind would indicate a surface ekman transport to the north, allowing for cooler waters to upwell near the southern shore – perhaps explaining the cooler SW layer. A NNW wind at Delta G would result in an ekman transport to the WSW, perhaps moving warmer surface waters to the southern shore. However, precise wind-ekman analysis like this is unlikely to hold, since the wind conditions directly in front of the glacier should be easterly katabatics (arising from cooled air on the glacier, moving towards the fjord, as we felt them while conducting the fieldwork). Additionally, the observed surface overflow (SO), particularly in the delta and upwelling overflow plumes (in the upper 1-5 m), is always moving towards the northwest. It is possible that the SW layer under the SO may move onshore/offshore depending on winds, but the three drogue measurements at about 20m depth (see Appendix A) indicate that directly under the turbid plume region, the flow is towards the north, along the ice face. This sort of analysis is hard to do without more robust wind and water velocity datasets. However, the point of this example (comparing Delta B and Delta G) is to illustrate that the water column stratification is significantly influenced by factors other than the tides (For more data, see Appendix A).

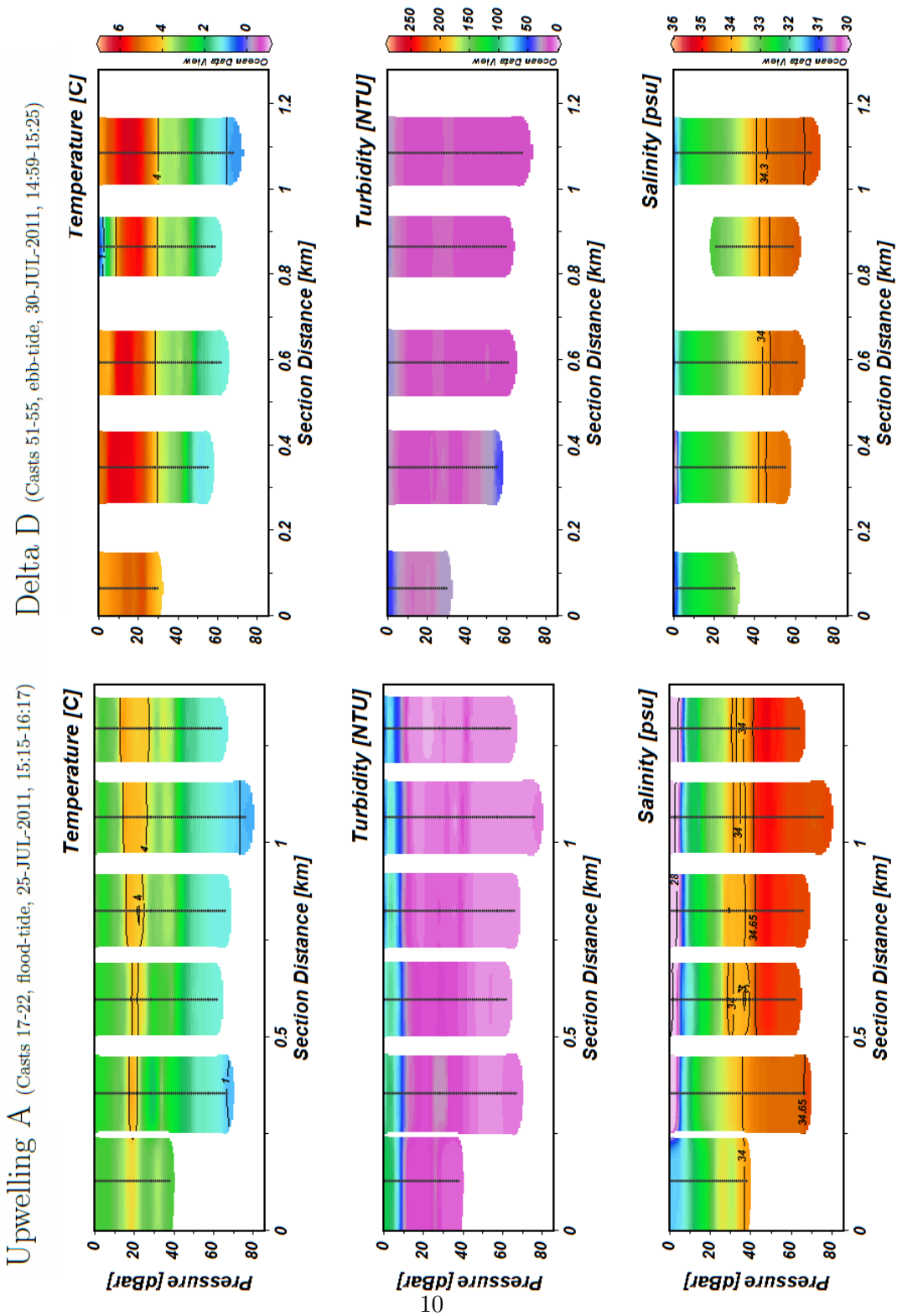


Figure 8: Here are two transects, Upwelling A and Delta D. Notice the turbidity structure in particular.

Ice Face Far (Casts 42-50, 75-79, high and ebb-tide)

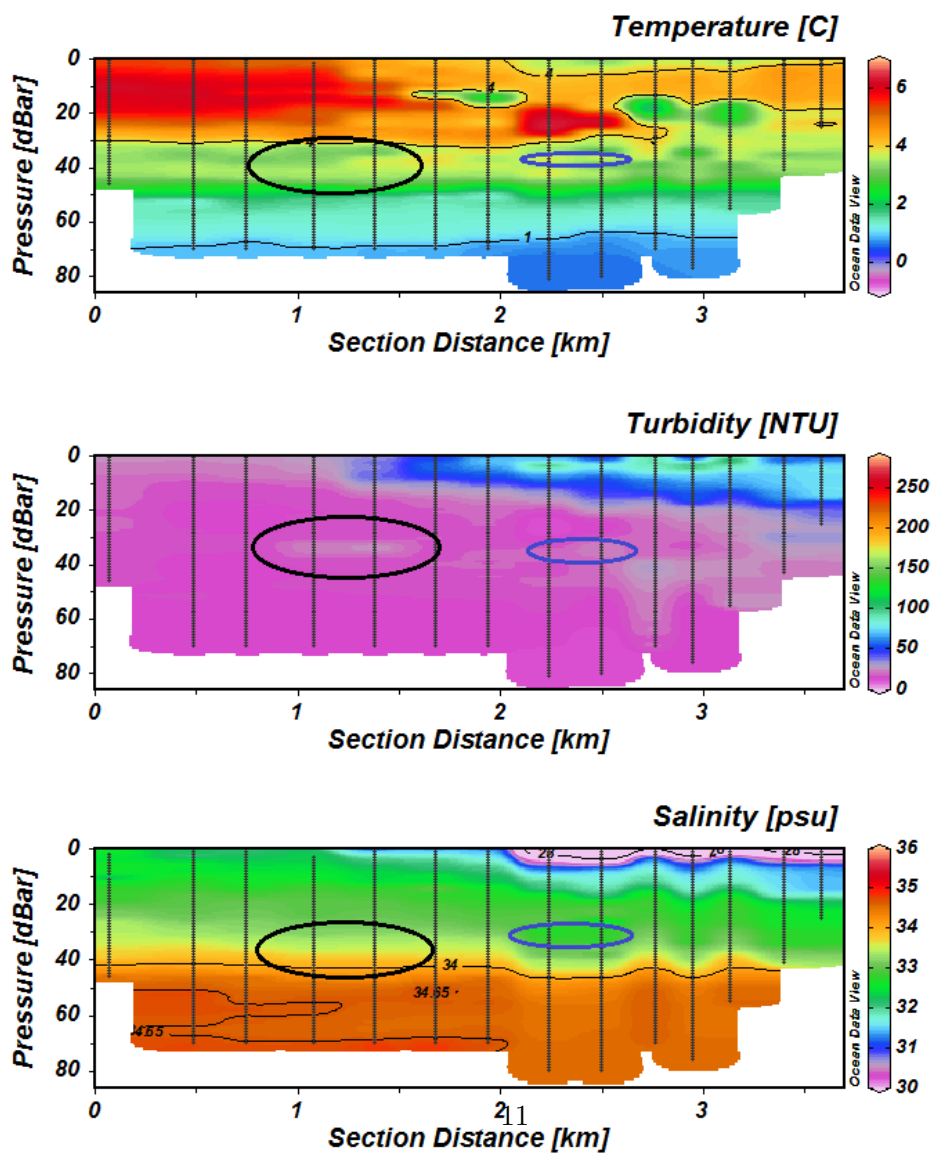


Figure 9: This transect is of Ice Face Far (see map). The region of the delta settling-out layer is circled in black. The blue circles indicate a very minor jump in temperature, which also corresponds with a dip in salinity and a rise in turbidity, that extends 1 to 2 m thick.

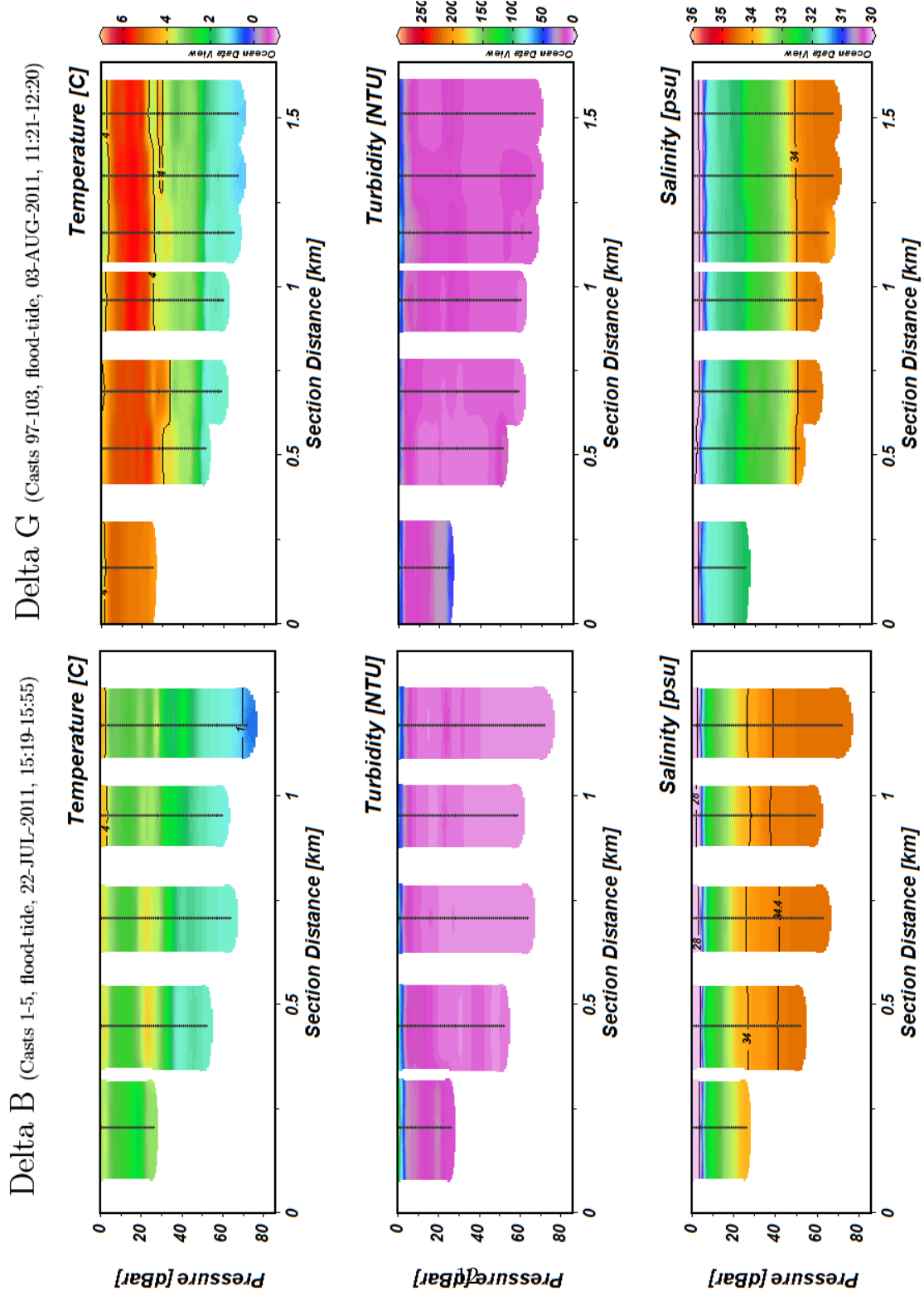


Figure 10: Here are two transects, Delta B and Delta G, both taken across the delta region during flood tide, at comparable hours of the day.

3.3 Interannual Variability

Despite the significant daily variability in the water column structure, there is a clear warming trend since 2005 (see Figure 11). While the temperature structure of the water masses is different between 2005 and 2011, the salinity structure remains comparable (see transects in Appendix B compared to those in Appendix A), suggesting a heat flux into the inner basin between 2005 and 2011 – and not necessarily a change in water mass origins/circulation itself.

4 Conclusions and Future Directions

There is significant daily variability in the water column structure in the inner fjord of Kongsfjorden, and there is no simple correlation between the variability and the tidal cycle. Local wind patterns and other prevailing weather conditions clearly play an important role in the oceanography here. Despite the daily variability, the data show a clear warming trend of about 2°C between 2005 and 2011, across the entire water column. Given that the 2009 REU group also observed warmer waters compared with 2005 (and it would certainly be worthwhile to make a scatter plot of the data from Hannah Marshburn’s 2009 REU thesis along with 2005 and 2011 data), it is likely that the heat flux originates with influx of TAW into the outer bay of Kongsfjorden (for example the 2006 prolonged intrusion noted by Willis et al., 2008 and Cottier et al. 2007). This indicates that the ice shelves in the inner basin of Kongsfjorden are susceptible to increased submarine melt due to TAW intrusions.

Further comparisons of known influxes of TAW into the outer fjord (from oceanographic cruises that have collected downfjord data) with the known interannual variability in the upper basin (from 2005, 2009, 2011 REU data) would be useful. Another possibility for future research in comparing the outer bay and inner basin would be to track water masses not only with physical oceanographic measurements but also with biotic community structure (e.g. Wang et al.’s 2009 work on plankton distribution – so perhaps collecting biological samples in the inner basin).

In terms of better-understanding the inner basin oceanography and its variability on the daily timescale, wind data closer to Kronebreen-Kongsvegen would be useful, as would water velocity profiles down the water column (for drogues can easily get stuck in eddies or icebergs and it is hard to determine if they are statistically significant).

In terms of further characterizing and modeling the inner basin oceanography based on the data presented in the appendices, it would be useful to more quantitatively explain the relationship between wind, tides, insolation, and water column structure. It would be worthwhile to use existing models of oceanography, with inputted parameters from meteorological or tidal data (e.g. Appendices C and D), and see if the outputs explain both the drogue/velocity measurements and the observed water column stratification (likely by comparing with σ from the salinity and temperature, but it would be good to first check

if the suspended sediment contribution to σ is significant by examining Trusel et al.'s calibration curves or the sediment sample weights from 2011, that Elizabeth Ceperley filtered and weighed). Another area for quantitative analysis would be examining the variability in the upwelling discharge (there is a good paper that models variations in the upwelling and melt rates: see Greisman 1979).

A very important area for further research is understanding the interannual variability in the water masses of Kongsfjorden. A strength of the Svalbard REU program is its ability to monitor these processes every two years. It would be very useful to continue collecting oceanographic data in the inner basin of Kongsfjorden in the future, and to see if this warming continues. It would also be useful to quantify the relationship between prevailing weather conditions and the inner fjord water column on the interannual scale (Julie and Ross mentioned that the 2011 summer was one of the mildest (sunny and warm) summers they had experienced at Ny Ålesund; might that be correlated to the heat flux in the oceanography?). That is, understanding the pathway of heat flux into the inner basin is useful; to what extent is heat transported through oceanographic mixing with TAW intrusions, and how important is the variability of meltwater, which is also dependent on insolation and air temperatures? A future oceanographic project might thus focus (rather than gearing the sampling strategy towards examining tidal variability) on studying the effects of winds and insolation on the water column structure or on understanding interannual variability of the water column.

5 References

1. Benn, D. I., C. R. Warren, and R. H. Mottram (2007). Calving processes and the dynamics of calving glaciers. *Earth-Science Reviews* 82:143-179.
2. Cottier, F. R., F. Nilsen, M. E. Inall, S. Gerland, V. Tverberg, and H. Svendsen (2007). Wintertime warming of an Arctic shelf in response to large-scale atmospheric circulation. *Geophysical Research Letters* 34, L10607, doi:10.1029/2007GL029948.
3. Cottier, F. R., V. Tverberg, M. E. Inall, H. Svendsen, F. Nilsen, and C. Griffiths (2005). Water mass modification in an Arctic fjord through cross-shelf exchange: The seasonal hydrography of Kongsfjorden, Svalbard. *Journal of Geophysical Research* 110, C12005, doi:10.1029/2004JC002757.
4. Elverhøi A., Ø. Lønne, and R. Seland (1983). Glaciomarine sedimentation in a modern fjord environment, Spitsbergen. *Polar Research* 1:127-149.
5. Greisman, Paul (1979). On upwelling driven by the melt of ice shelves and tidewater glaciers. *Deep-Sea Research* 26A:1051-1065.
6. Hasle, G. R., and B. R. Heimdal (1998). The net phytoplankton in Kongsfjorden, Svalbard, July 1988, with general remarks on species composition of arctic phytoplankton. *Polar Research* 17(1):31-52. Holland, D. M., R. H. Thomas, B. D. Young, M. H. Ribergaard, and B. Lyberth (2008). Acceleration of Jakobshavn Isbræ triggered by warm subsurface ocean waters. *Nature Geoscience* 1:659-664.
7. Kehrl, L. M., R. L. Hawley, R. D. Powell, and J. Brigham-Grette (2011). Glaciomarine sedimentation processes at Kronebreen and Kongsvegen glaciers, Svalbard. *Journal of Glaciology* 57(205):841-847.
8. Marshburn, H., R. Powell, J. Brigham-Grette. Glaciomarine oceanographic and suspended sediment dynamics, Kongsbreen system, Svalbard. Senior Thesis. University of Miami.
9. Motyka, R. J., L. Hunter, K. A. Echelmeyer, C. Connor (2003) Submarine melting at the terminus of a temperate tidewater glacier, LeConte Glacier, Alaska, U.S.A. *Annals of Glaciology* 36:57-65.
10. Nilsen, F., T. Gammelsrød, R. Skogseth (2011). Warm water reappears in Spitsbergen fjords. UNIS. Available: www.unis.no/60_NEWS/6070_Archive_2011/n_11_11_04_spitsbergen_fjords/warm_water_reappears_nwes_04112011.htm
11. Rignot, E., M. Koppes, and I. Velicogna (2010) Rapid submarine melting of the calving faces of West Greenland glaciers. *Nature Geoscience* 3:187-191.

12. Trusel L. D., R. D. Powell, R. M. Cumpston, and J. Brigham-Grette (2010). Modern glacimarine processes and potential future behaviour of Kronebreen and Kongsvegen polythermal tidewater glaciers, Kongsfjorden, Svalbard. *Geological Society London, Special Publications* 344:89-102, doi:10.1144/SP344.9.
13. Svendsen, H., A. Beszczynska-Møller, J. O. Hagen, B. Lefauconnier, V. Tverberg, S. Gerland, J. B. Ørbaek, K. Bischof, C. Papucci, M. Zajaczkowski, A. Roberto, O. Bruland, C. Wiencke, J.-G. Winther, and W. Dallmann (2002). The physical environment of Kongsfjorden-Krossfjorden, an Arctic fjord system in Svalbard. *Polar Research* 21:133-166.
14. Wang, G., C. Guo, W. Luo, M. Cai, and J. He (2009). The distribution of picoplankton and nanoplankton in Kongsfjorden, Svalbard during late summer 2006. *Polar Biology* doi: 10.1007/s00300-009-0666-6.
15. Willis K. J., F. R. Cottier, S. Kwaśniewski (2008). Impact of warm water advection on the winter zooplankton community in an Arctic fjord. *Polar Biology* 31:475-481.

6 Acknowledgements

I am very grateful to my advisor, Mary-Louise Timmermans. She is a wonderful advisor, and I will miss meeting her, working with her, and learning from her – and am so grateful I got to do all of those. My thanks to Sean Barrett, Peter Parker, and the Yale Physics Department for being very supportive of my interests and encouraging me to pursue research in the geological sciences. I am also very grateful to Ross Powell and Julie Brigham-Grette for mentoring me over the summer and for giving me the incredible opportunity to participate in and learn from the Svalbard REU program. My thanks to the rest of the fieldwork team, Elizabeth Ceperley, Daren McGregor, George Roth, Rebecca Siegel, Rachel Valletta, and Mark Goldner.

The Yale Center for Earth Observation (YCEO), directed by Ron Smith, is a research and teaching laboratory housed under the Yale Institute of Biospheric Studies (YIBS). I have done most of my data processing in the YCEO lab. My thanks particularly to Larry Bonneau, for very kindly installing extra software when needed. My thanks to the Yale Physics Department for funding travel to the 42nd International Arctic Workshop, where I received encouraging feedback on a poster presentation of this research. The fieldwork could not have been completed without the help of Norsk Polarinstitutt and Kings Bay, nor without generous funding from the National Science Foundation and the Yale Environmental Studies Summer Fellowship. My thanks also to Luke Trusel for sharing his raw data.

2011 Svalbard REU Oceanographic Data Report

Daksha M. Rajagopalan

20 May 2012

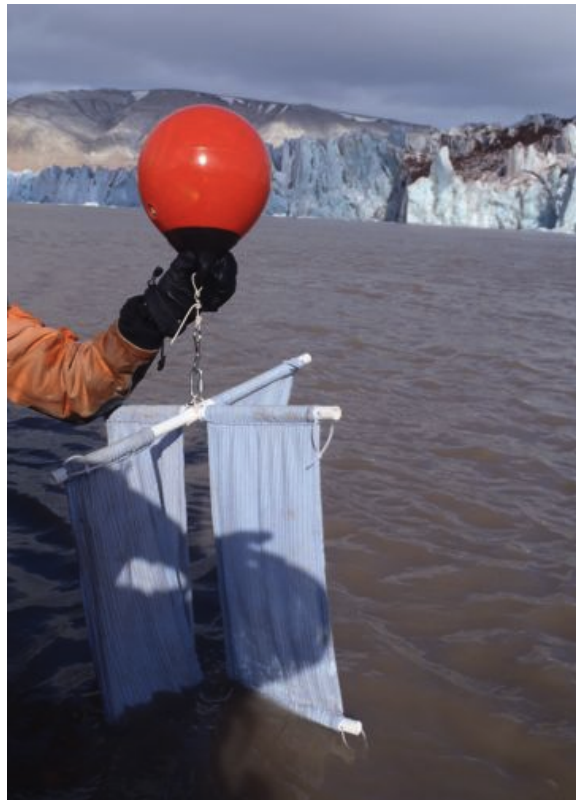
1 Introduction to the Fieldwork

Our data range from approximately 200 m to 1.5 km from the ice faces of Kronebreen and Kongsvegen, collected between 22 July and 6 Aug 2011 in Kongsfjorden, near Ny Ålesund in Svalbard. The survey site includes two glacial meltwater discharges. One, referred to as the "upwelling" is a subglacial meltwater stream that flows under Kronebreen, and mixes turbulently as it rises to the surface about 100 m from the glacier's calving front. Several birds feed where the upwelling reaches the fjord water surface, and the site of this upwelling can be identified by where the birds dive. The other significant glacial meltwater discharge occurs south of the upwelling. It is the discharge from Kongsvegen which flows from the Kongsvegen Delta. On the timescale of the study, the diurnal cycle and the tidal cycle have the largest effect on discharge fluctuations. We primarily used CTD devices with attached turbidity sensors to profile across key transects in the fjord, to capture the flood and ebb of the tide. We also constructed and deployed two lagrangian drifter buoys, drogued at various depths for an estimate of current velocity.

2 Drogue Data

2.1 Overview

The two drogues we used were constructed of a buoy attached by cord (of variable length: 1m, 20m, 40m, 50m) to a 'sail' composed of PVC piping and cotton bedsheet (See image below). We took 22 drogue measurements



in all. Each measurement consisted of noting the latitude and longitude of the release point, waiting a specific time interval, and recording the GPS location of the pick-up point. The data are presented here firstly in a table, then in maps with current directions. The distances were calculated from the latitude and longitude using `pos2dist.m` method 1 written by Langqiu Sun, shared on MATLAB Central's file exchange program (code included in Appendix E). It is unclear how representative these data are; the ocean is filled with eddies and it is possible for drogues to get caught in eddies. We took care to ensure drogues did not get caught in icebergs (for too long) by adjusting the few drogues that did get caught. It is important to note the tidal timing of the measurements; for example, all the drogue measurements at 50-m depth are at flood-tide. So these drogue data are not statistically significant, but they may still be useful. They are useful in two ways. Firstly, in calculating submarine glacial

meltrates, the surface drogues indicate the velocity of the upwelling plume against the ice face (see the Subglacial Stream Upwelling Velocity calculation in this Data Report); also, the velocities yielded by the drogues at 20 m and 40 m depth can also be used to refine the submarine meltrate calculation. Secondly, if further modeling of the oceanography is done (using weather, tide, and water density - from the CTD measurements - parameters), then the drogue measurements may serve as a check to the model's results.

Date	Run #	In		Out		distance
		Lat	Long	Lat	Long	
7/29	1	78.88658	12.52273	78.88855	12.51417	285.6825
7/29	2	78.86900	12.49045	78.87157	12.48790	290.9567
7/29	3	78.86867	12.48958	78.86960	12.48872	105.5137
7/29	4	78.88645	12.51907	78.88802	12.51975	174.8348
7/30	5	78.86857	12.49195	78.86885	12.49110	36.4024
7/30	6	78.88630	12.51800	78.88710	12.51177	160.4952
8/1	7	78.89353	12.47500	78.89370	12.48167	143.9334
8/1	8	78.89500	12.47390	78.89513	12.47387	14.8229
8/3	9	78.86813	12.49480	78.86968	12.49273	178.1595
8/3	10	78.87628	12.48370	78.87712	12.48390	92.9429
8/3	11	78.87582	12.48492	78.87642	12.48423	68.3854
8/3	12	78.88998	12.50902	78.89080	12.50612	110.1305
8/3	13	78.88668	12.52278	78.88863	12.51378	290.3211
8/3	14	78.88793	12.50630	78.88962	12.50628	187.4695
8/3	15	78.88778	12.50570	78.88845	12.50343	88.7196
8/3	16	78.88758	12.51203	78.88842	12.50957	106.8167
8/3	17	78.88693	12.51890	78.88892	12.52050	223.5091
8/8	18	78.89505	12.47370	78.89492	12.47628	57.2385
8/8	19	78.89502	12.47505	78.89513	12.47607	25.3112
8/8	20	78.88322	12.43316	78.88392	12.43150	85.6694
8/8	21	78.88387	12.43030	78.88422	12.42873	51.4336
8/8	22	78.88578	12.42262	78.88667	12.41997	113.61

Date	Run #	Time Duration (min)	duration (s)	Depth (m)	speed (m/s)	tide
7/29	1	0:11:00	660	1	0.43	high
7/29	2	0:14:25	865	1	0.34	High-ebb
7/29	3	0:04:31	271	1	0.39	High-ebb
7/29	4	0:05:45	345	1	0.51	ebb
7/30	5	0:06:10	370	1	0.10	ebb
7/30	6	0:07:10	430	1	0.37	ebb
8/1	7	0:39:55	2395	20	0.06	flood
8/1	8	0:40:07	2407	50	0.01	flood-high
8/3	9	0:09:57	597	1	0.30	ebb
8/3	10	0:23:52	1432	20	0.06	ebb
8/3	11	0:22:39	1359	40	0.05	ebb
8/3	12	0:04:37	277	1	0.40	ebb
8/3	13	0:10:52	652	1	0.45	Flood-high
8/3	14	0:37:24	2244	20	0.08	flood
8/3	15	0:33:13	1993	40	0.04	flood
8/3	16	0:33:23	2003	40	0.05	high
8/3	17	0:37:44	2264	20	0.10	High-ebb
8/8	18	0:16:22	982	20	0.06	flood
8/8	19	0:24:09	1449	50	0.02	flood
8/8	20	0:23:40	1420	20	0.06	flood
8/8	21	0:21:42	1302	50	0.04	flood
8/8	22	0:35:05	2105	50	0.05	flood

2.2 Surface



Figure 1: The lower cluster of drogues are in the delta region, and the upper cluster is in the upwelling overflow region. Drogues 1 to 6. 1 and 2 are in yellow, 3 and 4 are in blue, 5 and 6 are in white. The numbers indicate the starting point and the prime indicates the end point; for example, the yellow star labeled 1 is where drogue 1 was released; the yellow star labeled 1' is where drogue 1 was retrieved. Note that drogue 5 barely moved and has a much smaller velocity than the other surface drogues in the delta region; this might be due to daily variability in the delta discharge velocity (drogue 5 is the only surface, delta measurement for that day).



Figure 2: The lower cluster of drogues are in the delta region, and the upper cluster is in the upwelling overflow region. Drogue 9 is in pink, 12 is in blue, and 13 is in red.

2.3 20 m depth

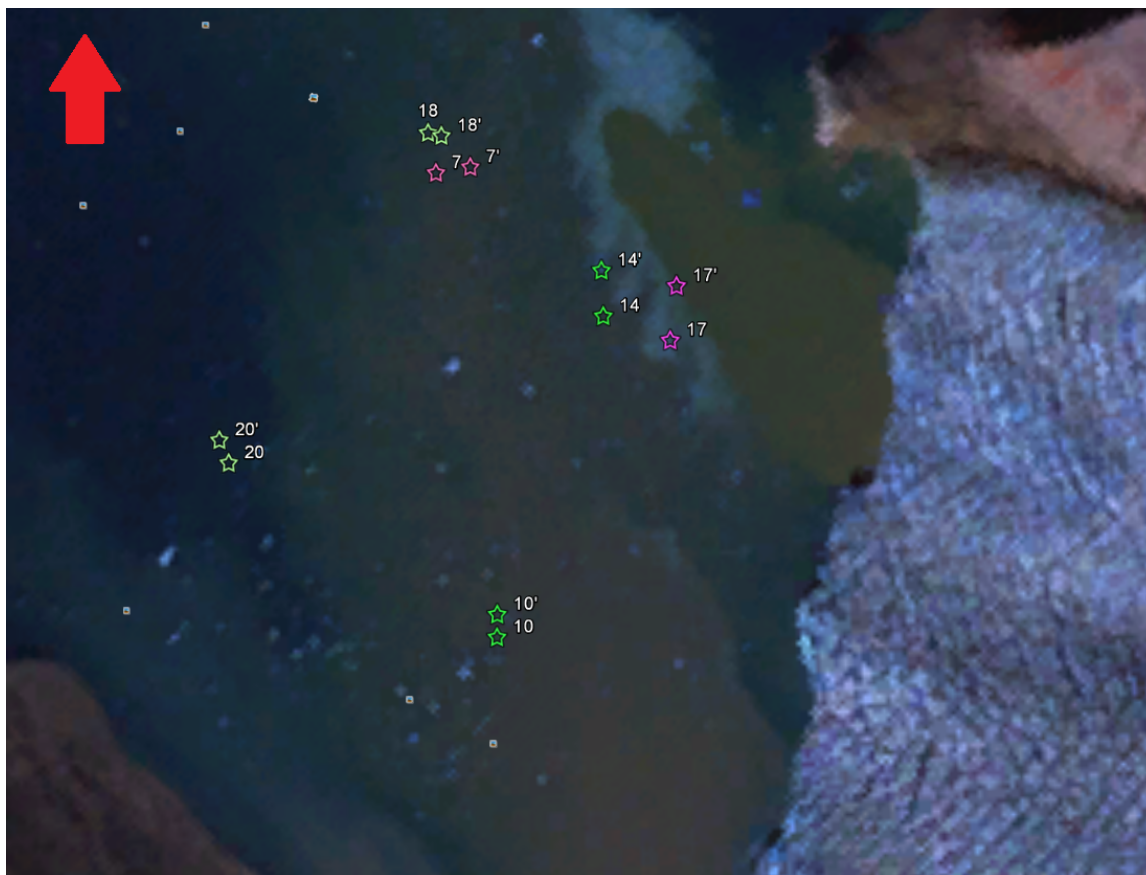


Figure 3: These drogues were suspended with a 20m-long rope between the surface buoy and the 'sail'. Based on these measurements, it appears that the water column at 20 m depth moves towards the north closer to the ice face (see drogue measurements 10, 14, 17). Farther out away from the ice face, at the southern shore of the fjord, the water is moving away from the ice face (see drogue measurement 20), and around the centerline of the fjord, the water is moving towards the ice face (see measurements 7, 18). Note that the three drogue measurements farther from the ice face (7, 18, 20) are all taken at flood-tide.

2.4 40 m depth



Figure 4: At 40m depth, closer to the ice face, the water column appears to be moving towards the northwest. Drogue 15 is in yellow, drogue 16 is blue, drogue 11 is red. The speed calculation for these drogues yield comparable values ($0.04 - 0.05 \frac{m}{s}$) and these numbers should be very useful in calculating submarine glacial melt rates. The three drogue measurements at 40 m (drogues 11, 15, 16) are at ebb, flood, and high -tide, respectively.

2.5 50 m depth



Figure 5: At 50 m depth, farther away from the ice face and at the centerline of the fjord, the water mass appears to be still (see drogue measurements 8 and 19, both at flood-tide). Along the southern shore of the fjord, the water is moving away from the ice face (see drogue measurements 21 and 22, both also at flood-tide). Drogue 8 is in peach, drogue 19 is in yellow. Drogue 22 is in white, drogue 21 is in yellow.

3 CTD and turbidity Data

We took 130 casts/profiles over the fieldwork period from 22 July to 6 Aug 2011.

3.1 Pre-Fieldwork: Instrument Specs and Calibration

We used two CTD instruments in the field, each with an attached turbidity sensor: Seabird SBE 19 (unpumped) with attached OBS Backscatterance, we call "Hans"; as well a pumped Seabird SBE 19plus V2 (strain-gauge pressure sensor), in a cage, and with attached OBS D&A 3+, we call "Gretel".

The instrument specifications and configurations as per Seabird's website and manuals, are as follows.

3.1.1 Specs for Gretel

	<i>Measurement Range</i>	<i>Initial Accuracy</i>	<i>Typical Stability</i>	<i>Resolution</i>
Conductivity (S/m)	0-9	0.0005	0.0003 S/m/month	0.00005 (most oceanic waters; resolves 0.4 ppm in salinity) OR 0.00007 (high salinity waters; resolves 0.4 ppm in salinity) OR 0.00001 (fresh waters; resolves 0.1 ppm in salinity)
<i>Temperature (°C)</i>	-5 to +35	0.005	0.0002 °C/month	0.00001
<i>Pressure – Strain-gauge</i>	100 meters	0.1 meter	0.1 meter/year	0.0002% of full scale range

Gretel was sampling at 4 Hz and was set to averaging every two measurements, so the raw data have a resolution of 2 Hz.

3.1.2 Specs for Hans

I am unable to locate Seabird's instrument specifications for the SBE 19. Hans was set to a sample rate of 2 Hz, so the raw data from both instruments have the same resolution: 2 Hz.

3.1.3 Config Files for Gretel

Here are the configuration files and numbers used for the SBE 19 plus V2 and OBS D&A 3+.

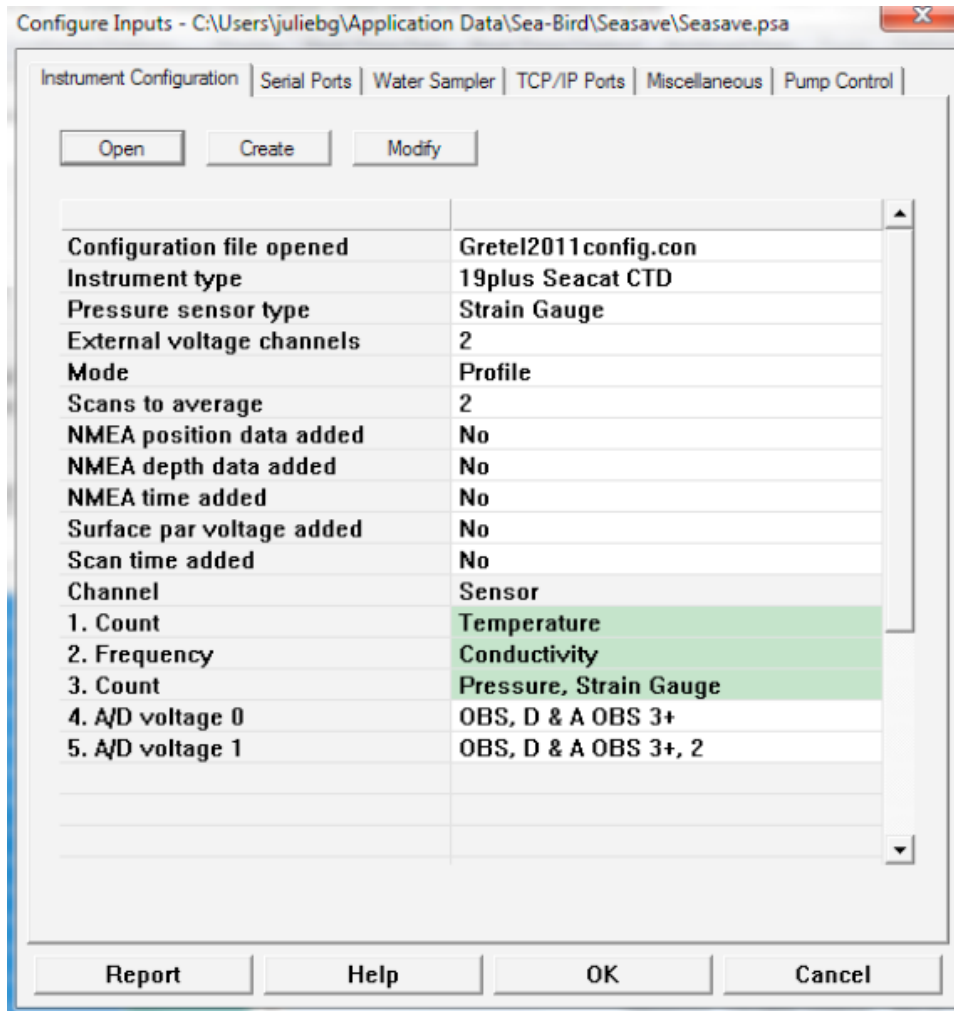


Figure 6: Main screen for Gretel in Seasave configuration menu

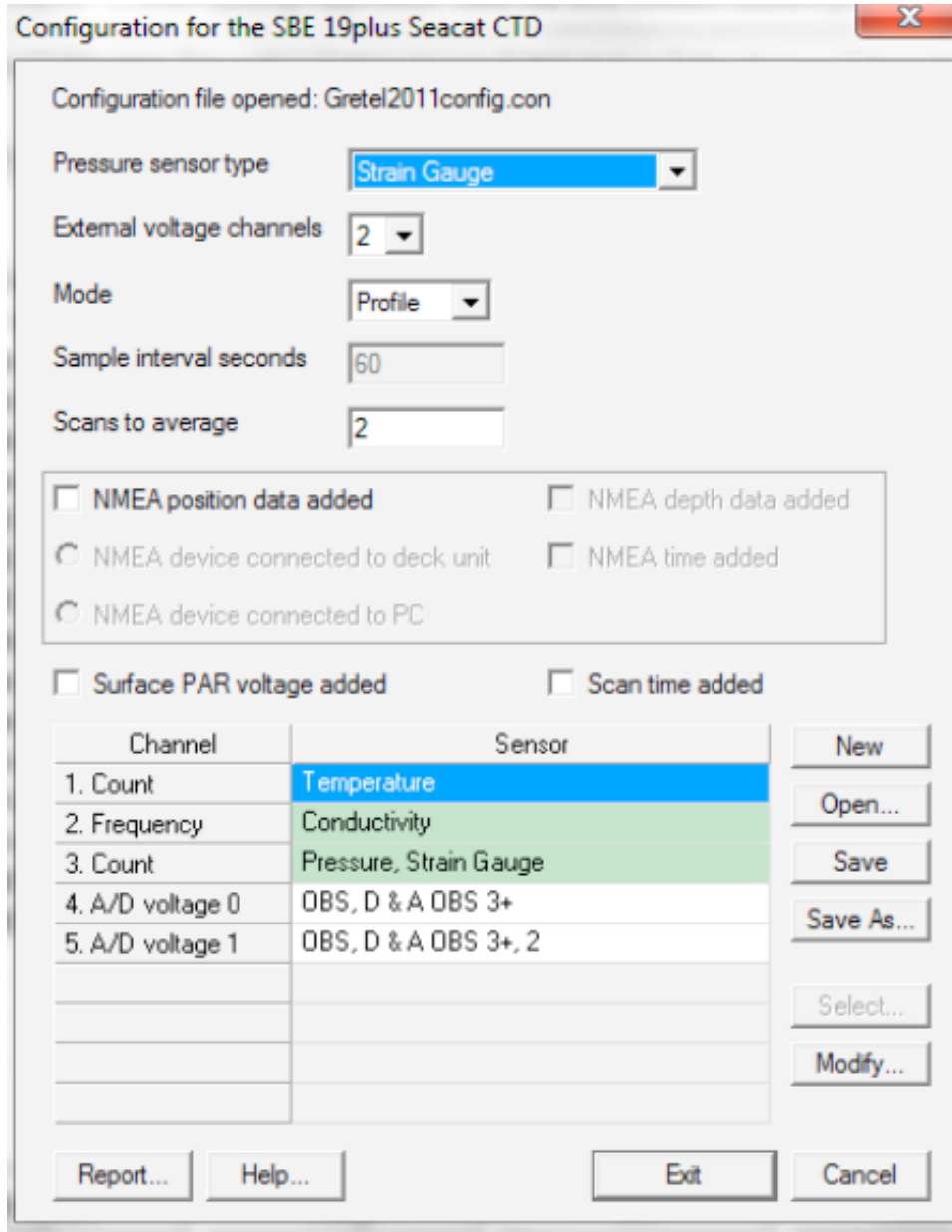
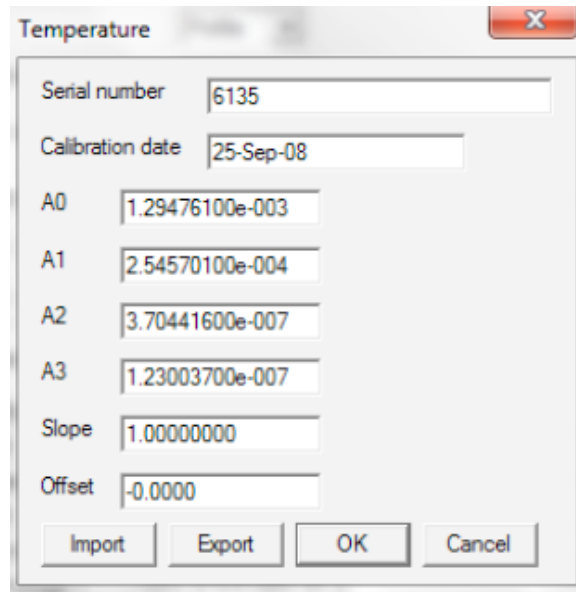


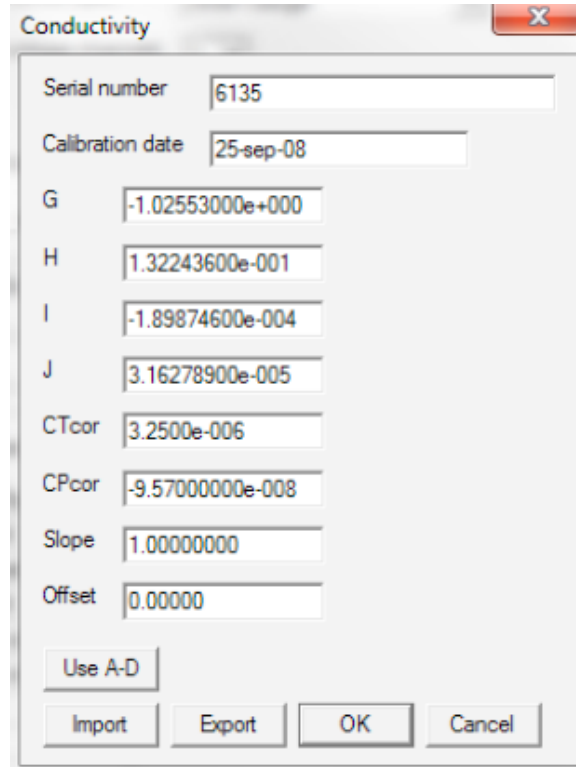
Figure 7: Note that Gretel has two OBS calibrations; one is for high turbidity, one is for low turbidity. (I do not recall now which one is which)



A dialog box titled "Temperature" with a close button (X) in the top right corner. It contains several input fields for calibration data. The fields are: Serial number (6135), Calibration date (25-Sep-08), A0 (1.29476100e-003), A1 (2.54570100e-004), A2 (3.70441600e-007), A3 (1.23003700e-007), Slope (1.00000000), and Offset (-0.0000). At the bottom, there are four buttons: Import, Export, OK, and Cancel.

Field	Value
Serial number	6135
Calibration date	25-Sep-08
A0	1.29476100e-003
A1	2.54570100e-004
A2	3.70441600e-007
A3	1.23003700e-007
Slope	1.00000000
Offset	-0.0000

Figure 8: 3



A dialog box titled "Conductivity" with a close button (X) in the top right corner. It contains several input fields for calibration data. The fields are: Serial number (6135), Calibration date (25-sep-08), G (-1.02553000e+000), H (1.32243600e-001), I (-1.89874600e-004), J (3.16278900e-005), CTcor (3.2500e-006), CPcor (-9.57000000e-008), Slope (1.00000000), and Offset (0.00000). At the bottom, there is a "Use A-D" button and four buttons: Import, Export, OK, and Cancel.

Field	Value
Serial number	6135
Calibration date	25-sep-08
G	-1.02553000e+000
H	1.32243600e-001
I	-1.89874600e-004
J	3.16278900e-005
CTcor	3.2500e-006
CPcor	-9.57000000e-008
Slope	1.00000000
Offset	0.00000

Figure 9: 4

Pressure, Strain Gauge

Serial number 6135

Calibration date 19-sep-08

PA0 2.19489900e-001

PA1 4.85688700e-004

PA2 -4.73705900e-012

PTEMPA0 -7.39759100e+001

PTEMPA1 5.25726100e+001

PTEMPA2 -5.26983700e-001

PTCA0 5.24202900e+005

PTCA1 3.72084100e+001

PTCA2 -7.33314600e-001

PTCB0 2.50760000e+001

PTCB1 8.00000000e-004

PTCB2 0.00000000e+000

Offset 0.000000

Import Export OK Cancel

Figure 10: 5

Configuration for the SBE 19plus Seacat CTD



Configuration file opened: Gretel2011config.con

Pressure sensor type: Strain Gauge

External voltage channels: 2

Mode: Profile

Sample interval seconds: 60

Scans to

NME
 NME
 NME
 Surfa

1. Count	
2. Frequ	
3. Count	
4. A/D voltage 0	OBS, D & A OBS 3+
5. A/D voltage 1	OBS, D & A OBS 3+, 2

Report... Help... Exit Cancel

New
Open...
Save
Save As...
Select...
Modify...

OBS, D & A OBS 3+

Serial number: T8415

Calibration date: 25-jun-08

A0: -0.328000

A1: 0.105900

A2: -1.603000e-006

Import Export OK Cancel

Figure 11: OBS

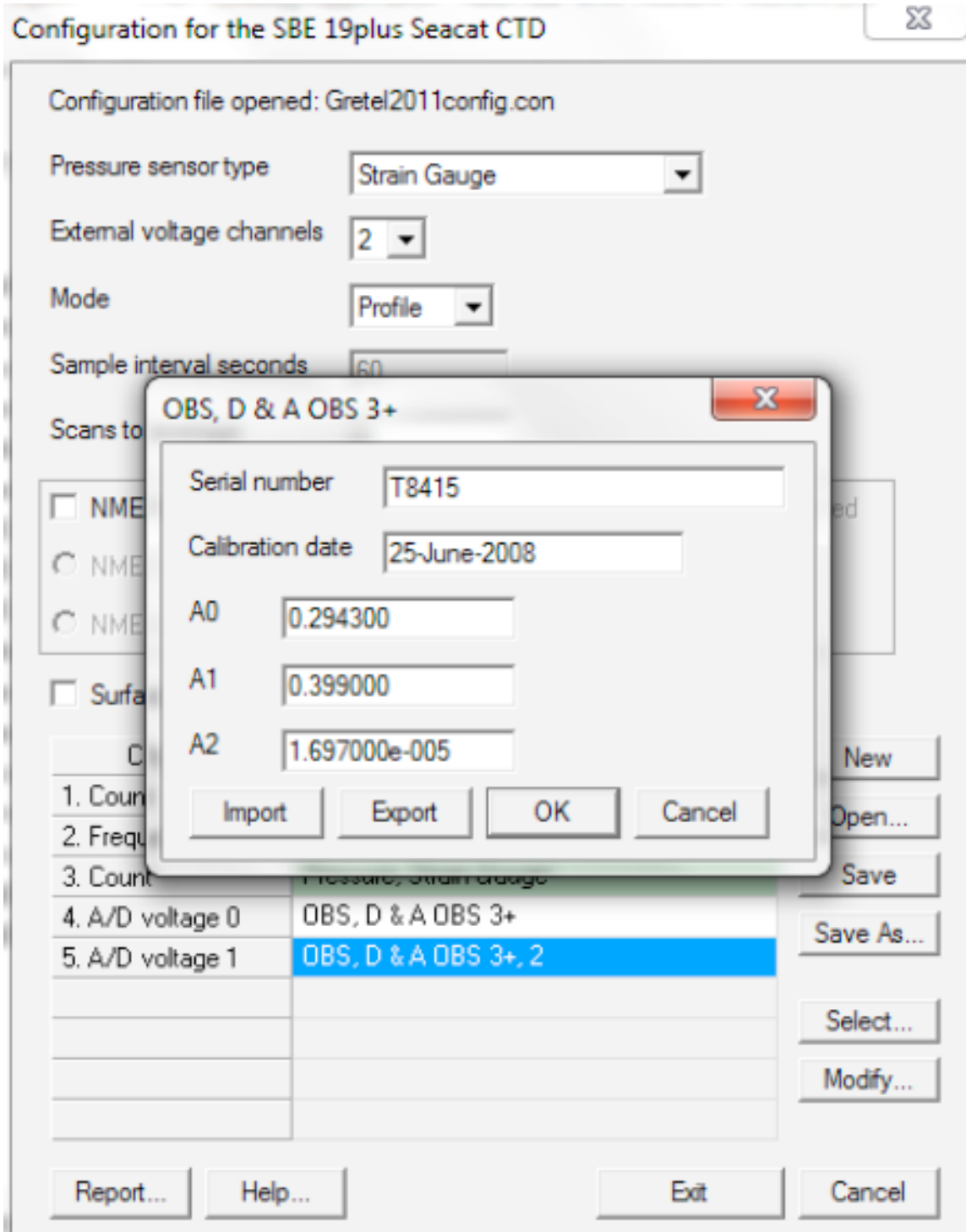


Figure 12: OBS

3.1.4 Config Files for Hans

Here are the configuration files and numbers used for the SBE 19 and OBS Backscatterance.

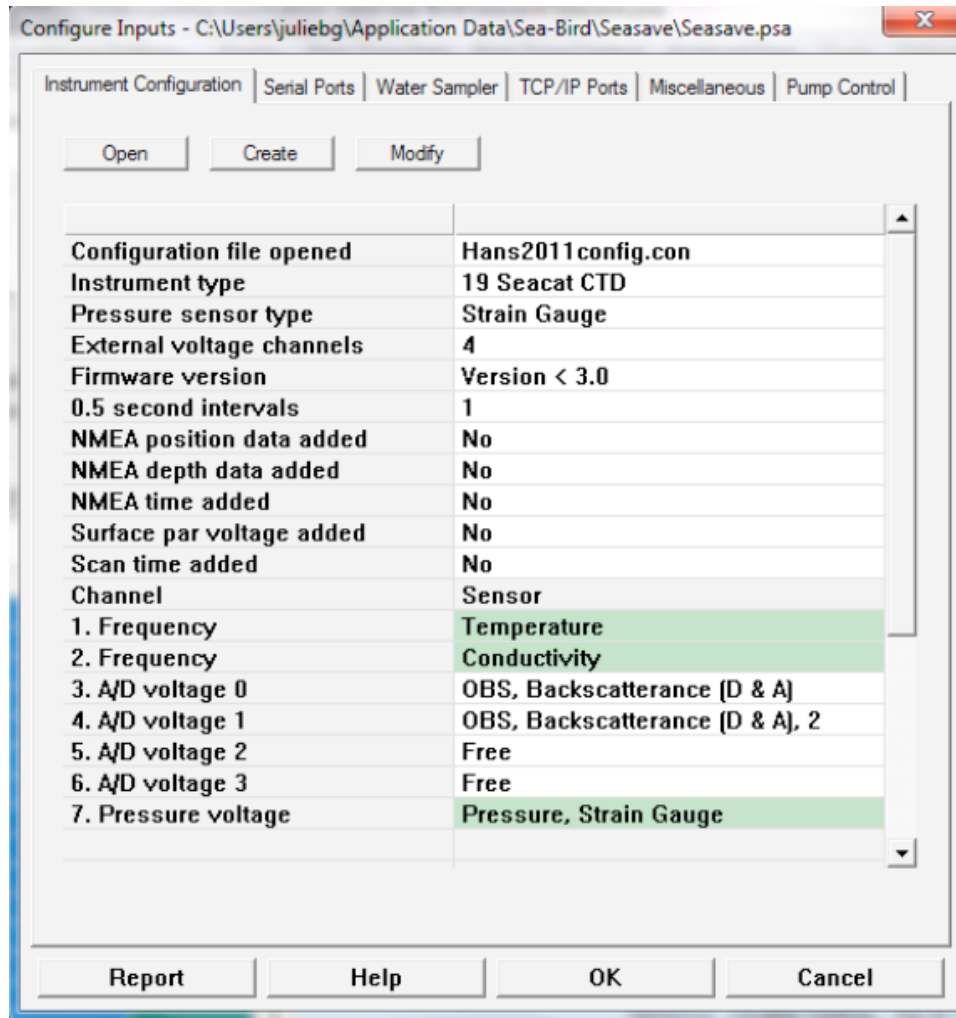


Figure 13: h1

Temperature

Serial number 508

Calibration date 10-Jun-08

G 4.15639162e-003

H 5.82702965e-004

I 2.26131087e-006

J -2.26261438e-006

F0 1000.000

Slope 1.00000000

Offset 0.0000

Use A-D

Import Export OK Cancel

Figure 14: h2

Conductivity

Serial number 508

Calibration date 10-Jun-08

G -4.05806261e+000

H 4.83487335e-001

I 1.40576236e-003

J -3.30857100e-005

CTcor 3.2500e-006

CPcor -9.57000000e-008

Slope 1.00000000

Offset 0.00000

Use A-D

Import Export OK Cancel

Figure 15: h3

OBS, Backscatterance (D & A)

Serial number 24227

Calibration date 05 sep 05

Gain 450.00

Offset 0.000

Import Export OK Cancel

Figure 16: h4

Pressure, Strain Gauge

Serial number 508

Calibration date 19-Jun-08

A0 5.046026e+002

A1 -1.302736e-001

A2 1.088177e-007

Offset 0

Import Export OK Cancel

Figure 17: h5

3.2 Fieldwork: Descent Rates and Resolution

Since the instruments were lowered on a manually operated winch, there is a lot of variation in the velocities. On average, the descent was approximately 0.37 m/s. With a sampling rate of 2 Hz, this results in vertical resolution of about 1.4 samples / meter. The minimum descent velocity over all the casts was 0.175 m/s, and the maximum was 0.6057 m/s. For an idea of how much variation there was in the velocities (just within each profile), below is a table of the average velocity (V_{avg} , meters/second) for each cast and the standard deviation (STD V) for that average. Also listed is vertical resolution (samples/meter). Notice that STD V for each cast is relatively large compared to V_{avg} .

Sheet1

Cast	Vavg	STD V	Vertical Resolution
average	0.3736	0.2146	1.4365
1	0.2141	0.1402	2.3350
2	0.2475	0.1606	2.0206
3	0.1750	0.1595	2.8578
4	0.1746	0.1599	2.8631
5	0.2261	0.1441	2.2118
6	0.2124	0.1244	2.3543
7	0.2352	0.0990	2.1261
8	0.2173	0.1012	2.3010
9	0.2444	0.1201	2.0456
10	0.2535	0.0958	1.9722
11	0.2718	0.1170	1.8393
12	0.2180	0.1408	2.2940
13	0.2533	0.1670	1.9738
14	0.2888	0.1268	1.7311
15	0.3635	0.2205	1.3754
16	0.3078	0.1217	1.6247
17	0.2213	0.1928	2.2594
18	0.3273	0.1518	1.5276
19	0.3346	0.1710	1.4942
20	0.3653	0.1600	1.3687
21	0.3692	0.1467	1.3543
22	0.3988	0.1476	1.2537
23	0.2739	0.2193	1.8258
24	0.2691	0.1686	1.8582
25	0.2495	0.1781	2.0038
26	0.3318	0.1575	1.5070
27	0.4260	0.1787	1.1737
28	0.4379	0.1227	1.1419
29	0.3433	0.2116	1.4564
30	0.2695	0.1015	1.8551
31	0.2595	0.1567	1.9267
32	0.3134	0.1302	1.5952
33	0.3415	0.1296	1.4640
34	0.3480	0.1251	1.4366
35	0.3455	0.1115	1.4470
36	0.3706	0.1467	1.3492
37	0.3694	0.1426	1.3534
38	0.2577	0.1964	1.9403
39	0.3281	0.1921	1.5239
40	0.3135	0.2224	1.5950
41	0.4420	0.2897	1.1313
42	0.3392	0.2181	1.4741
43	0.4024	0.2105	1.2425
44	0.3996	0.2212	1.2512
45	0.4747	0.2606	1.0533
46	0.5200	0.2194	0.9616
47	0.5258	0.2468	0.9509
48	0.4358	0.1850	1.1474
49	0.4390	0.2169	1.1389
50	0.3937	0.2583	1.2701
51	0.3724	0.2800	1.3428
52	0.4614	0.2346	1.0837
53	0.4568	0.1959	1.0947
54	0.3946	0.2378	1.2672

Sheet1

55	0.4408	0.1968	1.1342
56	0.3809	0.2404	1.3125
57	0.4543	0.2225	1.1005
58	0.4913	0.1767	1.0177
59	0.2956	0.2951	1.6914
60	0.6165	0.2625	0.8110
61	0.4981	0.3637	1.0038
62	0.4799	0.4025	1.0419
63	0.6323	0.2934	0.7908
64	0.4988	0.2787	1.0025
65	0.6057	0.2685	0.8254
66	0.5263	0.2250	0.9501
67	0.4385	0.2003	1.1402
68	0.4558	0.2030	1.0970
69	0.3937	0.2773	1.2700
70	0.3684	0.2795	1.3573
71	0.4861	0.2307	1.0287
72	0.3099	0.2985	1.6137
73	0.4847	0.2466	1.0316
74	0.3968	0.2690	1.2601
75	0.3962	0.2376	1.2619
76	0.4460	0.2209	1.1210
77	0.2706	0.2563	1.8477
78	0.3585	0.2876	1.3945
79	0.3639	0.2228	1.3741
80	0.4949	0.2545	1.0103
81	0.4662	0.2618	1.0725
82	0.4743	0.2520	1.0542
83	0.5093	0.2267	0.9818
84	0.4527	0.2344	1.1045
85	0.2702	0.1360	1.8503
86	0.4094	0.2465	1.2212
87	0.4057	0.2161	1.2324
88	0.3102	0.2420	1.6119
89	0.4259	0.2300	1.1740
90	0.5180	0.2198	0.9652
91	0.3500	0.2880	1.4285
92	0.4562	0.2158	1.0959
93	0.4129	0.2208	1.2111
94	0.4236	0.2077	1.1803
95	0.4362	0.2069	1.1462
96	0.4545	0.1919	1.1001
97	0.2928	0.1885	1.7076
98	0.3636	0.1803	1.3750
99	0.3591	0.1973	1.3925
100	0.3472	0.2109	1.4400
101	0.3798	0.2328	1.3166
102	0.3891	0.2060	1.2851
103	0.3479	0.2243	1.4372
104	0.1979	0.2319	2.5260
105	0.2483	0.2209	2.0138
106	0.3600	0.2139	1.3888
107	0.3403	0.2266	1.4694
108	0.3732	0.2446	1.3398
109	0.4246	0.2481	1.1776
110	0.4071	0.2919	1.2282

Sheet1

111	0.4718	0.2580	1.0598
112	0.3349	0.2363	1.4928
113	0.3389	0.2424	1.4753
114	0.3517	0.2631	1.4215
115	0.4004	0.2478	1.2488
116	0.4072	0.3005	1.2280
117	0.4408	0.2640	1.1342
118	0.1875	0.1926	2.6668
119	0.3426	0.1999	1.4596
120	0.4017	0.1784	1.2446
121	0.4050	0.1777	1.2346
122	0.3817	0.1774	1.3098
123	0.3773	0.2063	1.3253
124	0.3924	0.1855	1.2741
125	0.2969	0.2277	1.6839
126	0.4628	0.3575	1.0803
127	0.4755	0.3320	1.0515
128	0.4392	0.4342	1.1384
129	0.3516	0.3325	1.4222
130	0.2881	0.3296	1.7352

3.3 Post-Fieldwork: Data Processing

For each cast, I present two sets of data. The first is aligned, wildedited, and 1db bin-averaged. The second set is also processed as noted for each cast, but is otherwise the full-resolution data (not averaged, not aligned, not wildedited).

For the first data set:

First, I aligned the conductivity and temperature channels with respect to time. Since both instruments use temperature sensors with relatively slow response times, Seabird recommends advancing both temperature channels. For Gretel, Seabird recommends advancing temperature by +0.5 seconds and not advancing conductivity (since it is measured in a pumped chamber). For Hans, Seabird recommends advancing temperature by +0.5 seconds. For Hans, since the conductivity is measured in a cell whose flushing rate depends on descent rate, conductivity can either lag or lead temperature. However, for slow descent rates ($v \leq 0.75$ m/s), Seabird recommends advancing conductivity relative to temperature by 0 seconds.

I used SBE Data Processing's Align routine to advance T by +0.5 seconds for both Hans' and Gretels' profiles. I also advanced C by +0.5 seconds for Hans' profiles. Then, I used the Wildedit module to flag sudden spikes in all channels. Then I bin-averaged the profiles using a 1-db bin-size.

Additionally, once I imported the data into Ocean Data View, I individually edited some of the samples, as noted in the section containing each profile.

In the future, I suggest advancing temperature by more than +0.5 seconds for Gretel, since Seabird's recommended advance reduces—but does not eliminate—loops in the T-S diagrams. However, the appropriate advance value may be velocity dependent, so different advances may be required for different casts.

3.4 Profiles

(Refer to the separate file, appendixA2.pdf).